Vertically Edge-Oriented Graphene on Plasma Pyrolyzed Cellulose Fibers and Demonstration of Kilohertz High-Frequency Filtering Electrical Double Layer Capacitors

Nazifah Islam¹, Md Nadim Ferdous Hoque¹, Wenyue Li¹, Shu Wang², Juliusz Warzywoda³,

Zhaoyang Fan¹*

¹Department of Electrical and Computer Engineering and Nano Tech Center, Texas Tech University, Lubbock, TX 79409, USA

*Email: Zhaoyang.Fan@ttu.edu (Zhaoyang Fan)

Abstract

High-frequency electrochemical capacitors or electrical double layer capacitor (HF-ECs) with large capacitance were developed from edge-oriented graphene (EOG) nanosheets perpendicularly grown around carbonized cellulose microfiber (CMF) sheets. Binder-free EOG/CMF electrodes were fabricated in a one-step 5-min plasma-enhanced chemical vapor deposition process, where cellulose fiber sheets were rapidly pyrolyzed by high-temperature plasma, while EOG simultaneously formed on the developing CMFs. Owing to combined unique characteristics of both EOG and CMF, such facilely produced electrodes exhibit excellent performance in terms of both high frequency response and high capacitance density. In aqueous electrolyte cells, 10 μm thick EOG/CMF electrode exhibits an areal capacitance of 1.07 mF cm⁻² at 120 Hz along with a frequency of 13.8 kHz at –45° phase angle. ~ 3 V organic electrolyte cells show an areal capacitance of 0.49 mF cm⁻² at 120 Hz, and a frequency of 1.47 kHz at –45° phase angle. Developed HF-ECs were successfully applied in practical applications as ripple current filter in line-frequency AC/DC conversion, and as pulse power storage/smoother in environmental energy harvesting for self-powered micro devices.

²Department of Nutritional Sciences, Texas Tech University, Lubbock, TX 79409, USA

³Materials Characterization Center, Whitacre College of Engineering, Texas Tech University, Lubbock, TX 79409, USA

1. Introduction

There has been great interest in the study and development of ultrafast electrochemical capacitors (ECs) with response in kilohertz high frequency range, aiming to substitute them for the commonly used aluminum electrolytic capacitors (AECs) for current ripple filtering, [1-3] pulse power storage and generation, [4] and other similar functions. AECs have a low capacitance density, and their bulky size limits the downscaling of DC power modules and circuit boards for slim, compact and wearable electronics.[5] ECs have a larger capacitance density than AECs by several orders of magnitude; however, a maximum working frequency of conventional ECs is typically lower than 1 Hz.[6, 7] They are only suitable as energy sources but not as conventional capacitors for filtering at high frequencies. Therefore, a performance gap exists between ECs and AECs in terms of frequency response and capacitance density. It has been envisioned that if high-frequency ECs (HF-ECs) with a compact size could be developed for filtering applications as the substitution for bulky AECs, circuit board form could be further scaled down for slim, small and light electronics. For the most common filtering application in the line-frequency AC/DC conversion, considering the harmonic frequencies, such HF-ECs should be able to respond in kilohertz (kHz) range.

Steady progress is being made toward developing kHz HF-ECs by tailoring different nanocarbon-based electrodes,[3, 4, 8-16] prominently oriented graphene, carbon nanotube thin films, carbon nanofiber aerogel, and many others.[2] One key issue to achieve high frequency response is to minimize the equivalent resistance. This requires a minimized interfacial resistance between the current collector and the carbon material, high conductivity of the carbon material, and rapid electrolyte ion migration in the porous carbon electrode. Minimizing the electrode material resistance is critical by using highly conductive carbon materials, while tailoring the

porous structure is equally, if not more important. Based on de Levie's porous electrode model, the pore has a time constant $\tau = \frac{1}{4}z^2RC$, where z is the pore penetration depth, R and C are the pore resistance and capacitance per unit length.[17] This constant is further deduced as $\tau \propto z^2/d$, where d is the pore diameter. Clearly, high frequency response, or small pore time constant requires shallow pores and large pore size. Therefore, tailoring nanocarbon electrode structure by minimizing or eliminating micropores or even mesopores has been particularly interesting.

Achieving kilohertz response while maintaining large areal and volumetric capacitance densities for HF-ECs is a challenging goal. Usually, a high frequency response comes at the expense of low capacitance density since micropores and mesopores in the electrode must be sacrificed. Fast ECs have been obtained from a variety of carbon-based nanomaterials, but either their capacitance density is small or their frequency response is limited.[18-20] Another challenge for HF-ECs is their low operation voltage. Most studies explored aqueous electrolyte-based cells to achieve high-frequency response because aqueous electrolytes exhibit high ionic conductivity; however, such cells have a potential window smaller than 1 V, and this significantly limits their practical applications. HF-ECs with vertical graphene and organic electrolyte was first reported in [21]. Detailed presentation of frequency dependent behavior and other device characterizations were later on reported in [9, 10].

Herein, aiming at achieving both high response frequency in kHz range and a large capacitance density, as well as a wider voltage window, we investigated edge-oriented multilayer graphene (EOG) network grown on carbonized cellulose microfiber (CMF) sheets, which were used as a binder-free electrode for development of kilohertz frequency HF-ECs, as illustrated in Fig. 1. Both aqueous electrolyte cells and organic electrolyte cells are reported. The rationale to adopt such an EOG/CMF electrode is based on the following considerations.

In terms of tailoring the pore structure of an electrode for high frequency response, vertically oriented multilayer graphene (VOG) on a flat surface,[1] which is produced in a plasma enhanced chemical vapor deposition (PECVD) process, with its fully exposed graphene edges and oriented channels between graphene sheets, seem to be an ideal electrode structure for kHz HF-ECs. As schematically highlighted in Fig. 1b: (1) the aligned multilayer graphene sheets are rooted in the surface or subsurface of the substrate with a trivial interfacial resistance; (2) graphene sheets have reasonably large conductivity; (3) the aligned channels between sheets allow electrolyte ions to migrate rapidly for charge and discharge; and (4) the fully exposed graphene edges and steps can be easily accessed by electrolyte ions as adsorption sites. For this last point, it should be emphasized that the capacitance at the edge plane is much larger than at the basal plane.[22] However, on a flat substrate, the achievable VOG surface area is limited, resulting in a small areal capacitance density, and therefore oriented graphene network grown perpendicularly around a 3D porous scaffold, i.e. EOG, was further investigated.[23, 24]

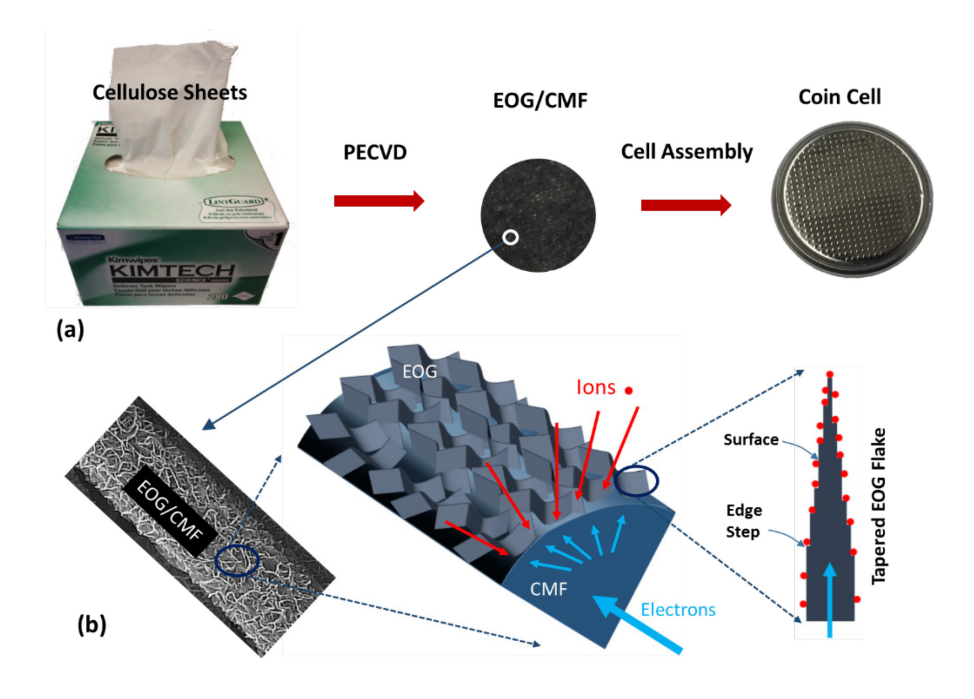


Fig. 1. Schematics illustrating (a) the one-step process from cellulose paper to EOG/CMF binder-free electrode, which was then studied in a coin cell, and (b) EOG network on carbon fiber with fully exposed graphene edges along the tapered perpendicular graphene sheet for easy access, and inter-sheet channels facilitating rapid electrolyte transport.

The conventional carbon cloth is too thick to be used as a 3D scaffold for HF-ECs. Here, we carbonized very thin cellulose wiper sheet into 10 µm thick carbon microfiber sheet for use as the 3D scaffold for EOG deposition. As the most common polymer and a renewable resource with large scale annual production, cellulose fibers are being exploited as carbon fiber precursor for electrochemical energy storage due to their abundance, low-cost, and high content of carbon. [25, 26] Time- and energy-consuming thermal pyrolysis of polymer fiber sheets at high temperatures for several hours or even longer, in an inert or active gas environment, is commonly applied to obtain carbon fiber sheets with abundant micro- and meso-porous structures, [27-30] which, however, are not suitable as electrodes for HF-EC. For this study, in a 5-minute rapid PECVD process, EOG nanosheets with fully exposed graphene edges were grown perpendicularly wrapped around carbon microfibers, which were rapidly formed by pyrolysis of cellulose microfibers in the same PECVD process to minimize micropore generation (Fig. 1a). Plasma pyrolysis is a technique used to produce high quality carbon fiber networks from natural or artificial polymer fibers, and has previously been identified as a key process for producing highly conductive non-porous carbon fibers for HF-ECs.[4, 31]

With thus-formed ~10 μ m thick EOG/CMF sheets used as freestanding electrodes, we demonstrated aqueous electrolyte cells that had a –45° phase angle frequency (f_0) of 13.8 kHz, and an areal capacitance density of 1.07 mF cm⁻² at 120 Hz (C_A^{120}), which corresponds to 120 Hz

volumetric density of 1.07 F cm⁻³ when considering the whole volume of the electrode. We further boosted the operation voltage to \sim 3V by using organic electrolyte, and these organic electrolyte cells had a frequency of 1.47 kHz at -45° phase angle and C_A^{120} of 0.49 mF cm⁻². As a proof of concept, we applied these HF-ECs as a substitution for AECs for ripple current filtering in line-frequency AC/DC conversion, and for pulse power storage/smoothing used in environmental mechanical energy harvesting.

2. Experimental methods

Conventional cellulose wiper (KimwipesTM) sheet was used as the cellulose material. During PECVD process, the chamber pressure was maintained at 30 torr with gas flow rates of H₂ and CH₄ controlled at 100 sccm and 50 sccm, respectively. The molybdenum stage, loaded with cellulose sheets, was electrically heated to 750 °C for a few minutes. The plasma was then ignited by 1 kW microwave power to deposit EOG around carbonized microfiber surfaces. The growth was continued for only 5 min. For comparison, bare CMF was also produced by carbonizing cellulose paper under the same conditions as described above, except that cellulose sheets were covered with graphite foils to prevent direct exposure to plasma species in avoiding EOG deposition.

X-ray diffraction analysis of cellulose paper and EOG/CMF was carried out using a Bruker AXS D5005 X-ray diffractometer. Microstructures of CMF and EOG/CMF were observed using a Hitachi H-9500 transmission electron microscope. Chemical composition and bonding states in cellulose paper and EOG/CMF were analyzed using a PHI 5000 VersaProbe X-ray photoelectron spectrometer. Raman spectra of CMF and EOG/CMF were obtained using a Bruker Optics SENTERRA dispersive Raman spectrometer.

Electrochemical characterization of the CMF and EOG/CMF electrodes was performed in both aqueous (6 M KOH in deionized water) and organic (1 M TEABF4 in anhydrous acetonitrile) electrolytes. Filter paper was used as a separator in aqueous electrolyte-based cells; commercial Celgard 2325 was used as a separator in organic electrolyte-based cells. The electrodes and separators were soaked in electrolytes for several hours. CR2016 type coin cells were assembled using symmetric electrodes. For organic cells, assembling was carried out in an Ar-filled glovebox with moisture and oxygen content less than 0.1 ppm. Electrochemical measurements were conducted using a Biologic SP 150 electrochemical workstation. Electrochemical impedance spectroscopy (EIS) was measured in the range of 100 kHz to 1 Hz with a sinusoidal AC voltage of 10 mV amplitude. Cyclic voltammetry (CV) was carried out in 0–0.8 V range for aqueous cells, and in 0–2.5 V range for organic cells at different scan rates ranging from 1 V s⁻¹ to 1 kV s⁻¹.

3. Results and discussion

3.1 Material characterization

In a PECVD process with methane and hydrogen as precursors, graphene flakes can vertically grow on a 2D flat surface. Methane molecules were cracked in the plasma, and the activated carbon species deposited on the substrate. Several possible factors might coordinately result in the vertical sheet growth on the flat substrate. [32-35] Firstly, the growth rate is always much higher in the sheet plane along the edge than in the sheet stacking direction due to bonding force difference, and it is further enhanced by hydrogen etching effect. Therefore, carbon radicals arriving at the top edges of sheets, either by directly diffusing from the gas phase or by surface migration, will be easily bonded along the edge to expand the sheets. Secondly, low angle sheets are starved for active carbon species because they are overshadowed and blocked by the fast-

growing vertical sheets. Thirdly, the vertical electrical field in the plasma sheath might also play a role. Now if a 3D scaffold, instead of a flat surface, is used as the growth substrate, as long as the scaffold is submerged in the plasma, the plasma sheath will form around the scaffold, and the active species in the plasma will impinge on the scaffold surface from different directions. Thus, EOG can grow perpendicularly wrapped around a porous 3D scaffold[14, 36] via the same mechanisms as on a flat substrate.

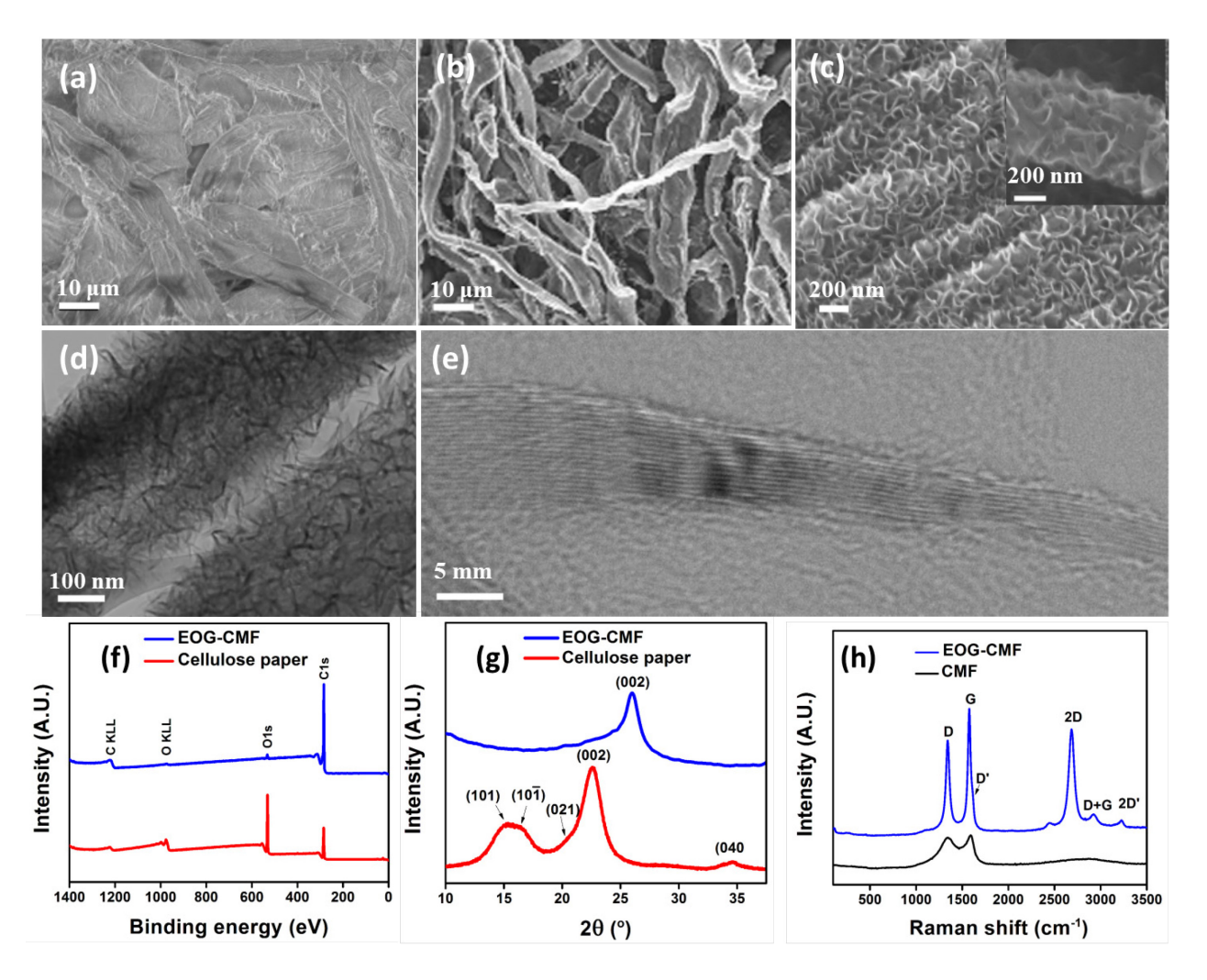


Fig. 2. (a) SEM image of the unwoven cellulose paper. (b, c) SEM images of EOG sheets grown on CMF. (d) Low and (e) high magnification TEM images of EOG sheets. (f) XPS survey spectra

of cellulose paper and EOG/CMF. (g) XRD patterns of cellulose paper and EOG/CMF. (h) Raman spectra of cellulose paper carbonized in plasma (CMF) and EOG/CMF.

The morphology of cellulose wiper sheet, carbonized cellulose fiber sheet, and edge-oriented graphene sheets grown around the fibers were analyzed by scanning electron microscopy (SEM) and transmission electron microscopy (TEM). Cellulose paper used is made of 100% virgin wood fiber. The SEM image in Fig. 2a reveals that the unwoven cellulose paper consists of the ribbonshaped cellulose fiber bundles with a width up to $\sim 10 \mu m$, and these bundles form a relatively compact structure at the microscale. The ribbon shape of the fiber bundle was probably caused by a compressing force during the paper manufacture. Each bundle consists of many small cellulose fibers. Pure cellulose is a homopolysaccharide composed of β-D-glucopyranose units, with all carbon atoms oxidized. After pyrolysis, with the majority of O and H released, cellulose fiber is reduced into carbon fiber. The area of carbonized fiber sheet decreases to $\sim 20\%$ of the initial area of cellulose wiper sheet, and large spacings appear between neighboring fiber bundles. As shown in Fig. S1 in the Supplementary Information (SI), each carbon fiber bundle in CMF sheet maintains the micrometer scale ribbon shape, but the sub-micrometer scale to nanometer scale carbon fibers could also be identified (Fig. S2). The macroscale morphology of EOG/CMF sheet is similar to that of CMF sheet (Fig. 2b vs. Fig. S1). The undulating microscale morphology of EOG flake networks (Fig. 2c), which perpendicularly grow on the underlying carbon fibers with a thickness of $\sim 0.5 \mu m$ (the inset of Fig. 2c), is caused by these underlying individual small carbon fiber bundles. Circling of individual fibers by EOG nanosheets was observed by both SEM (the inset of Fig. 2c), and TEM (Fig. 2d), which revealed that individual EOG flakes are perpendicularly wrapped around each carbon fiber. High-resolution TEM (Fig. 2e) revealed that each EOG flake

consists of multiple atomic layers of graphene. The tapered EOG flake has a wider base and a narrower tip, thus the atomic layer step edges are distributed along the vertically oriented EOG wall, and are fully exposed to allow easy access by an electrolyte. Fig. S3, showing sharp tips of EOG flakes, further confirms this point. These exposed step edges, together with the in-plane surfaces, act as effective adsorption sites for ions, thus forming double layer capacitance.

Elemental compositions and crystalline structures were elucidated for these materials. Elemental analysis, based on X-ray photoelectron spectroscopy (XPS) spectra shown in Fig. 2f, reveals a high oxygen concentration in cellulose compared to that in the EOG/CMF sample, owing to the significant oxygen loss during the high-temperature plasma pyrolysis. This demonstrates the effectiveness of plasma pyrolysis despite its short 5-min duration. X-ray powder diffraction (XRD) patterns in Fig. 2g show the crystalline structures of cellulose paper and EOG/CMF sheet. Wood fiber contains cellulose I_{β} , which consists of parallel chains forming hydrogen-bonded sheets that stack with an alternating shear parallel to the axis of the chain stabilized by van der Waals interactions. This crystalline structure has a monoclinic unit cell. The observed five peaks in the XRD pattern can be well indexed to cellulose I_B (101), (10 $\overline{1}$), (021), (002), and (040) planes.[37] In contrast, after plasma pyrolysis, XRD pattern of CMF (not shown) has a very broad peak and no sharp features, while the pattern of EOG/CMF exhibits a sharp peak at 26.0° 2θ, which is superimposed on the broad background peak. This sharp peak is due to (002) graphene, while the broad feature is caused by the largely amorphous carbon fibers formed by pyrolysis of cellulose fibers. The amorphous characteristic of CMF is further observed by HRTEM, which shows the predominantly amorphous carbon structure with small domains exhibiting irregular graphite features (Fig. S4). The different crystalline characteristics of CMF and EOG are further revealed by Raman spectra in Fig. 2h, where EOG sample exhibits the characteristic D (1342 cm⁻¹), G

(1576 cm⁻¹), D' (1614 cm⁻¹), 2D (2685 cm⁻¹), D+G (2922 cm⁻¹), and 2D' (3226 cm⁻¹) bands of multilayer graphene. The relatively strong defect-related D peak in this sample comes from fully exposed high-density edges. This is further confirmed by the appearance of shoulder D' peak of the G band that is due to graphene sheet edge effect.[8, 38] In contrast, CMF sample shows much weaker and broader peaks that suggest its dominant amorphous nature. Thus, Raman spectroscopy also reveals significant structure-related differences between the amorphous carbonized cellulose fiber and the highly-ordered graphene structure.

3.2 Aqueous cell studies

The electrochemical capacitive properties of EOG/CMF electrodes were first investigated using a coin cell structure with two symmetric electrodes in 6 M KOH solution utilized as an aqueous electrolyte. Cyclic voltammetry (CV) scans were performed at different scan rates up to 1,000 V s⁻¹. Representative CV curves are presented in Fig. 3a. At such high scan rates, cells maintained the desired rectangular-like response, revealing their high-frequency response capability. Voltage dependent capacitance densities at different scan rates are derived from corresponding CV data. As shown in Fig. S5, the quasi-rectangular shape suggests a near constant capacitance in the voltage window investigated. In particular, the plots at different rates overlap each other, indicating little loss of capacitance even at a very high scan rate of 1000 V s⁻¹.

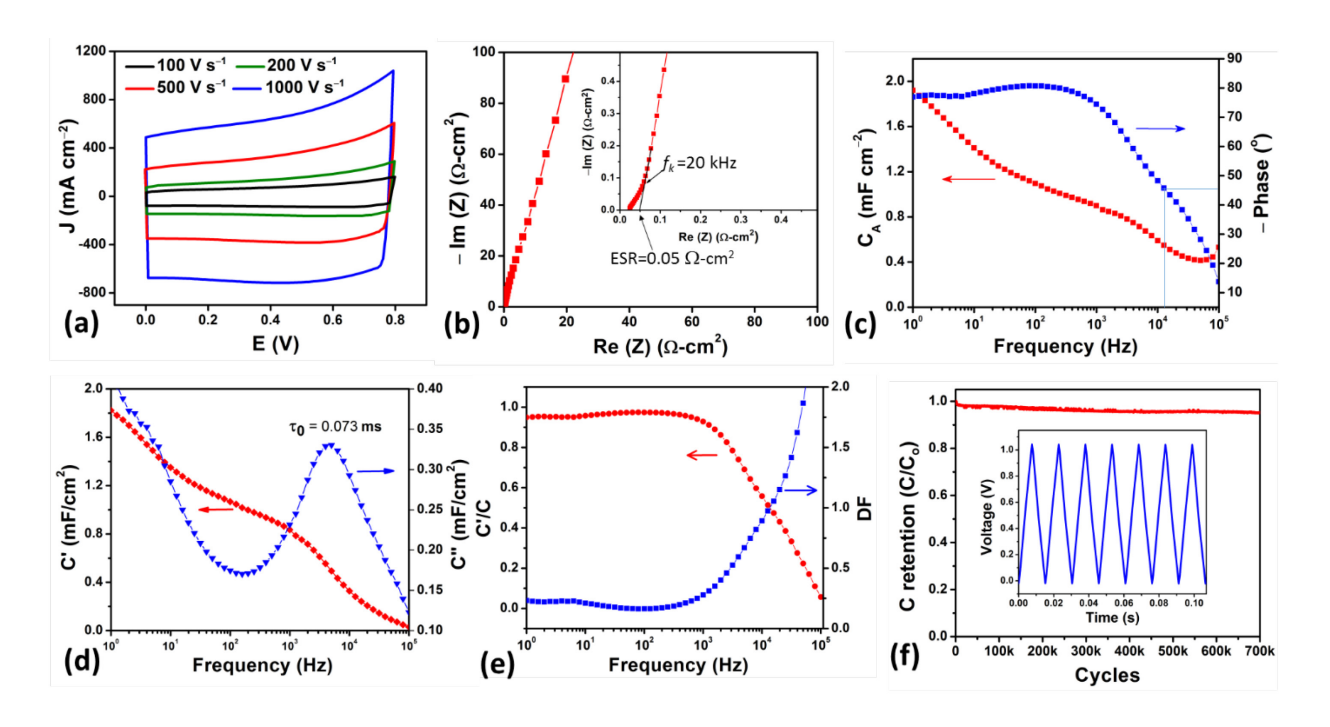


Fig. 3. Aqueous electrolyte-based EOG/CMF HF-EC performance. (a) Cyclic voltammetry plots at different scan rates up to 1000 V s⁻¹. (b) Nyquist complex impedance spectrum, with the inset showing the zoom-in of the spectrum in the high frequency range. (c) Areal capacitance density derived from EIS spectrum, and the Bode phase spectrum. (d) Areal capacitance density (C') derived from the complex capacitance C. The C" plot indicates the relaxation time of 0.073 ms. (e) Ratio of C'/C and the dissipation factor. (f) Galvanostatic cycling at 20 mA cm⁻² for 700,000 cycles with representative C-D curves shown as the inset.

The high-speed response of these cells is further revealed in electrochemical impedance spectroscopy (EIS) studies. The Nyquist complex impedance plot (Fig. 3b) is nearly linear with a large slope at low frequencies, which can be modeled as a constant phase element (CPE). A knee point appears at higher frequencies, corresponding to a knee frequency (f_k) of ~ 20 kHz, followed by a very small characteristic 45° slope region, but no clear semicircle region is observed. Since the 45° slope region is caused by the distributed resistance and capacitance in porous structure

[39], the observed very small region of this feature above 20 kHz suggests that the porous effect in the EOG/CMF electrode is not apparent until above this frequency. This is ascribed to two factors. Evidently, the spacing between neighboring graphene walls in the oriented EOG does not result in the porous effect, and the unique rapid plasma pyrolysis process used to carbonize cellulose paper does not produce a high concentration of nanopores. By minimizing the porous effect, a large knee frequency of 20 kHz was measured. Below this frequency, the cell can be modeled as a CPE in series with an equivalent series resistor (ESR). Considering the large slope of the spectrum to be close to a vertical line, the ideality factor of the CPE can be approximated as 1; and thus, the CPE becomes a capacitor. From the spectrum in Fig. 3b, a total ESR of 0.05 Ω ·cm², which includes the equivalent distributed resistance, was derived. Such a small ESR value is due to the high conductivity of the EOG/CMF material and its minimized porous effect, and is necessary for the cell to respond at a high frequency with a minimal power loss.

The areal electrode capacitances were extracted using a simplified RC model, and are plotted against frequency in Fig. 3c. At 120 Hz, the EOG/CMF electrode exhibited an area capacitance as high as 1.07 mF cm⁻². This value is larger than values reported previously employing edge-oriented or vertical graphene as electrodes.[8, 14, 21, 24, 40, 41] It is noted by combing carbon black with VOG, higher capacitance of ~ 2 mF cm⁻² was reported.[42] Considering that the free-standing EOG/CMF electrode has an approximate thickness of 10 μ m, a volumetric capacitance of 1.07 F cm⁻³ was derived at 120 Hz.

The EIS spectrum is further plotted in the Bode phase format (Fig. 3c). An ideal capacitor has a phase angle of -90° . Our cell exhibits a phase angle with its absolute value close to or above 80° in the relevant frequency range between 100 - 1000 Hz. This suggests resistive loss is small in this frequency region. Specifically, at 120 Hz, the cell showed a phase angles of -80.5° .

Assuming a simple series *RC* model, the frequency when the phase angle reaches –45° defines the boundary between capacitive impedance dominance and resistive impedance dominance, and above this frequency the cell becomes more lossy.[43] From Fig. 3c, a frequency at –45° phase angle of 13.8 kHz was found for our EOG/CMF aqueous cell.

Electrical behavior of the double layer capacitors formed at EOG/CMF electrodes was further analyzed using the concept of complex capacitance. An areal specific complex electrode capacitance is defined as $C(\omega) = C'(\omega) - jC''(\omega)$, where $C'(\omega)$ corresponds to the actual areal capacitance, and $C''(\omega)$ stands for areal specific power losses due to resistive effects as well as leakage currents, which are collectively represented by the frequency dependent resistance as observed by the impedance spectroscopy.[44, 45] $C'(\omega)$ and $C''(\omega)$ are plotted in Fig. 3d. From $C'(\omega)$, an electrode capacitance of ~ 1.05 mF cm⁻² is obtained at 120 Hz. This is in agreement with the value calculated based on the series-RC model in Fig. 3d. The evolution of $C''(\omega)$ with frequency reaches a maximum at the at -45° phase angle frequency that defines the relaxation time constant τ_0 . Fig. 3d shows that $C''(\omega)$ reaches a maximum at the -45° phase angle frequency of 13.7 kHz (consistent with the result obtained from Fig. 3c), which gives a relaxation time constant of 0.073 ms.

In the concept of complex capacitance, the ratio of C'/C reveals the ideality of the capacitor. It is observed from Fig. 3e that at lower frequencies ($< \sim 1\text{-}2 \text{ kHz}$), C'/C approaches 1, indicating capacitor's ideality in this range. Furthermore, based on the C' and C'' values, the reactive and real power components, |Q| and |P|, were derived (see SI)[45], and the ratio, |P|/|Q|, defined as dissipation factor (DF), is also potted in Fig. 3e. The small DF reveals the small loss characteristic in the low frequency range ($< \sim 1\text{-}2 \text{ kHz}$).

The performance stability is another critical figure of merit for filtering HF-ECs. It is known that for ripple filtering applications, the charge-discharge (C-D) depth of the filtering capacitor is small so that the voltage on this capacitor has no obvious change, thus having an almost constant DC output. Here, we tested EOG/CMF-based aqueous cells in galvanostatic C-D mode at a current density of 20 mA cm⁻² for up to 700,000 cycles, but with 100% discharge depth for accelerated failure test. The capacitance retention with C-D cycles is illustrated in Fig. 3f, with the inset showing the C-D curves for a few representative cycles. The capacitance retention is more than 94% after 700,000 cycles of 100% discharge depth, suggesting our EOG/CMF electrode based HF-EC is stable with long lifetime. The complex impedance plot of the cell before and after 700,000 cycles is provided in Fig. S6. The impedance curve shows slight increase in resistance, which might be caused by evaporation of an electrolyte.

3.3 Organic cell studies

The merit of aqueous cells is their high speed due to high conductivity of aqueous electrolyte.[46] Therefore, most reports on HF-ECs have been based on aqueous electrolytes.[12, 40, 41] However, their low operating voltage window, typically limited to 0.8 V, hampers their practical filtering applications. The allowable operating voltage range is much wider, up to ~ 3 V, in organic electrolytes. Thus, organic cells of EOG/CMF electrodes with 1 M TEABF4 in anhydrous acetonitrile solution[47] were also studied.

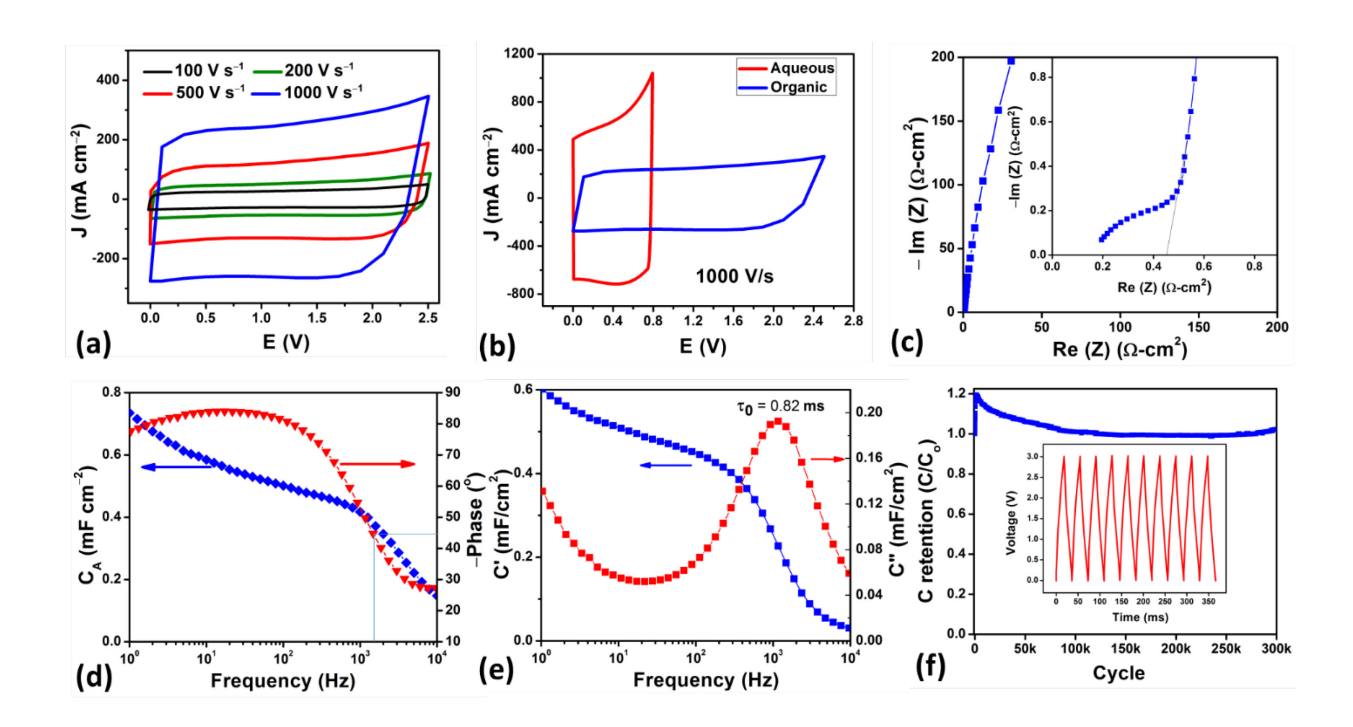


Fig. 4. (a) Organic electrolyte-based EOG/CMF HF-EC performance. (a) Cyclic voltammetry curves at several scan rates. (b) Comparison of CV curves at 1,000 V s⁻¹ rate for aqueous and organic electrolytes. (c) Nyquist complex impedance spectrum, with the inset showing the zoomin of the spectrum in the high frequency range. (d) *RC* model-derived areal capacitance and the Bode phase spectrum. (e) Real and imaginary components of the complex capacitance. (f) Galvanostatic cycling at 50 mA cm⁻² for 300,000 cycles.

CV scans were performed with scan rates up to 1,000 V s⁻¹. The CV curves at selected scan rates are presented in Fig. 4a. The organic cell maintained the desired quasi-rectangular shape even at a rate of 1,000 V s⁻¹, indicating its high-speed capability. The current densities at different scan rates (Fig. S7) show a linear relationship, indicating a desired capacitive behavior even at very high scan rates. Voltage dependent capacitance densities at different scan rates are derived from the corresponding CV, and are plotted in Fig. S8. The quasi-rectangular shape of plots shown in Fig. S8 suggests a near constant capacitance in the voltage window investigated. In particular,

plots obtained at different rates overlap each other, indicating little loss of capacitance in such a large scan rate range. For comparison, CV curves at 1,000V s⁻¹ for both aqueous and organic cells, based on the same EOG/CMF electrode structure, are plotted in Fig. 4b. It is noted that when using organic electrolyte, the voltage window significantly widened, while the electrode capacitance was somewhat reduced.

The low ionic conductivity of organic electrolyte will impact cell's frequency response. From the Nyquist plot of complex impedance of the organic cell (Fig. 4c), it is observed that at a high frequency a small semicircle feature appears, and the knee frequency is reduced to 3.8 kHz. The larger distributed resistance results in a larger total ESR of $\sim 0.45~\Omega \cdot \text{cm}^2$. Using the series RC model, the electrode capacitance at different frequencies was calculated (Fig. 4d). At 120 Hz, this capacitance is found to be 0.49 mF cm⁻², half of that of the aqueous cell. Based on the analysis of the Bode phase plot of the EIS spectra (Fig. 4d), the organic cell exhibits 120 Hz phase angles of -80.4° , suggesting a reasonably small loss at this high frequency, even though the -45° phase angle frequency is reduced to 1.47 kHz. Using the analysis based on the complex capacitance, the electrode capacitance (C') was also calculated (Fig. 4e), and values similar to those shown in Fig. 4d were obtained. Fig. 4e also shows that $C''(\omega)$ reaches a maximum at a frequency ~ 12.2 kHz, giving a relaxation time constant of 0.82 ms. C'/C and DF plots are shown in Fig. S9.

To examine the cycling life of organic cells, galvanostatic cycling for 300,000 cycles was performed at 50 mA cm⁻² current density, and results are presented in Fig. 4f. For organic cells, the capacitance increases to a very high value at the beginning, but eventually settles down close to the initial value, maintaining almost 100% capacitance retention for a long cycling duration. The initial jump is likely to be caused by electrode wetting, as in case of organic electrolyte, the low surface tension and high viscosity leads to slower electrode wetting. The electrodes were not

pre-conditioned for wetting in this study. The capacitance stabilizes after 100,000 cycles. The complex impedance curves of the cell before and after 100,000 cycles are presented in Fig. S10. The ESR does not show noticeable change, but the DC resistance increases slightly.

3.4 Application demonstration

As a proof of concept, we tested the EOG/CMF-based HF-EC for ripple current filtering in 60 Hz line-frequency AC/DC conversion (Fig. 5a). Organic cells were used due to their much higher voltage threshold compared to aqueous cells. A 60 Hz sinusoidal voltage was supplied as the input by a function generator, with a 4 V amplitude (Fig. 5b). The sinusoidal input passes through a full-bridge rectifier and then is buffered by the HF-EC as the filtering capacitor. Thus obtained DC output is supplied to a load. As shown in Fig. 5c, a ripple-free steady output voltage of 2.8 V was obtained after rectification and filtering. This suggests compact HF-ECs could be applied as a substitution for bulky AECs for such applications.

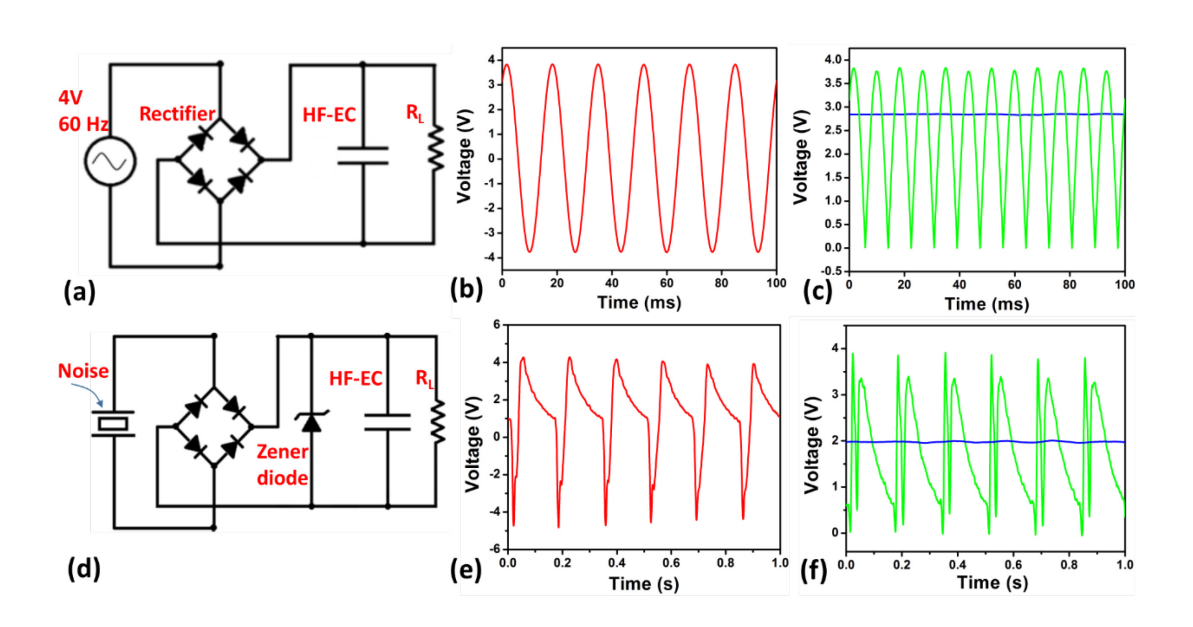


Fig. 5. (a-c) Demonstration of AC/DC conversion using a HF-EC as the filtering capacitor: circuit diagram (a), input 60 Hz sine wave (b), and the output from the rectifier without filtering (green curve) and the smooth DC output when using HF-EC filter (blue line) (c). (d-f) Demonstration of pulse power storing/smoothing using a HF-EC: circuit diagram (d), the pulse from the piezoelement (e), and the output from the rectifier without smoothing (green curve) and the constant DC output with HF-EC smoothing (blue line) (f).

Another emerging application area of HF-ECs is storage and smoothing of power pulses harvested from environmental vibration via piezo- or tribo-generators to power small autonomous devices that operate without external power supply.[48] Most miniaturized temperature, pressure or other sensors operate in 2–3 V limit and draw a current in microampere range. In order to simulate a microwatt load similar to that of these sensors, a 2 M Ω load resistor was chosen. The circuit shown in Fig. 5d was used for this demonstration, where a piezoelectric element was used to pick up environmental vibration and convert it to electric pulses. As the pulses from the piezo generator can be as large as 20 V depending on the intensity of mechanical vibration, a 3 V Zener diode was placed in parallel to the HF-EC to clamp the applied voltage in its safety window. Irregular voltage pulses (Fig. 5e) generated by mechanical vibrations from a piezo element are rectified and passed through the HF-EC. A smooth voltage of ~ 2 V was achieved across the load resistor (Fig. 5f). Such a system can be utilized to power low voltage micro-sensors and similar autonomous devices.

4. Conclusion

High-frequency EDLCs based on aqueous and organic electrolytes and their applications for current ripple filtering and pulse power storage were demonstrated. A one-step 5-min CH₄/H₂ plasma process was used to carbonize cellulose wiper sheet into carbon microfiber sheet, and to simultaneously grow edge-oriented graphene network perpendicularly around these microfibers. Thus obtained EOG/CMF freestanding electrode with a thickness of 10 μm was demonstrated to be an excellent structure for HF-ECs. In aqueous cells, the large electrode areal and volumetric capacitance densities of 1.07 mF cm⁻² and 1.07 F cm⁻³ at 120 Hz were demonstrated, along with a frequency of 13.8 kHz at −45° phase angle. We further boosted the operating voltage of HF-EC to ~ 3 V by using an organic electrolyte, which exhibited a −45° phase angle frequency of 1.47 kHz. This organic electrolyte-based EOG/CMF HF-EC was successfully used as a filtering capacitor for line-frequency AC filtering to achieve smooth DC output in AC/DC conversion, and as a pulse storing/smoothing capacitor in environmental mechanical energy harvesting systems.

Acknowledgements

This work was supported by National Science Foundation (1611060).

References

- [1] J.R. Miller, R.A. Outlaw, B.C. Holloway, Graphene double-layer capacitor with ac line-filtering performance, Science 329 (2010) 1637-9.
- [2] Z. Fan, N. Islam, S.B. Bayne, Towards kilohertz electrochemical capacitors for filtering and pulse energy harvesting, Nano Energy 39 (2017) 306-320.
- [3] K. Sheng, Y. Sun, C. Li, W. Yuan, G. Shi, Ultrahigh-rate supercapacitors based on eletrochemically reduced graphene oxide for ac line-filtering, Sci. Rep. 2 (2012) 247.

- [4] N. Islam, S. Li, G. Ren, Y. Zu, J. Warzywoda, S. Wang, Z. Fan, High-frequency electrochemical capacitors based on plasma pyrolyzed bacterial cellulose aerogel for current ripple filtering and pulse energy storage, Nano Energy 40 (2017) 107-114.
- [5] J. Both, Electrolytic Capacitors From the Postwar Period to the Present, IEEE Electr. Insul. M. 32(2) (2016) 8-26.
- [6] L.L. Zhang, X.S. Zhao, Carbon-based materials as supercapacitor electrodes, Chem. Soc. Rev. 38(9) (2009) 2520-2531.
- [7] Y. Zhu, S. Murali, M.D. Stoller, K. Ganesh, W. Cai, P.J. Ferreira, A. Pirkle, R.M. Wallace, K.A. Cychosz, M. Thommes, Carbon-based supercapacitors produced by activation of graphene, Science 332(6037) (2011) 1537-1541.
- [8] M. Cai, R.A. Outlaw, R.A. Quinlan, D. Premathilake, S.M. Butler, J.R. Miller, Fast Response, vertically oriented graphene nanosheet electric double layer capacitors synthesized from C₂H₂, ACS Nano 8(6) (2014) 5873-82.
- [9] Y. Yoo, S. Kim, B. Kim, W. Kim, 2.5 V compact supercapacitors based on ultrathin carbon nanotube films for AC line filtering, J. Mater. Chem. A 3(22) (2015) 11801-11806.
- [10] Y.J. Kang, Y. Yoo, W. Kim, 3-V Solid-State Flexible Supercapacitors with Ionic-Liquid-Based Polymer Gel Electrolyte for AC Line Filtering, ACS Appl. Mater. Interfaces 8(22) (2016) 13909-17.
- [11] Q. Zhou, M. Zhang, J. Chen, J.D. Hong, G. Shi, Nitrogen-Doped Holey Graphene Film-Based Ultrafast Electrochemical Capacitors, ACS Appl. Mater. Interfaces. 8(32) (2016) 20741-7.
- [12] Z. Zhang, M. Liu, X. Tian, P. Xu, C. Fu, S. Wang, Y. Liu, Scalable fabrication of ultrathin free-standing graphene nanomesh films for flexible ultrafast electrochemical capacitors with AC line-filtering performance, Nano Energy 50 (2018) 182-191.
- [13] D. Premathilake, R.A. Outlaw, R.A. Quinlan, S.G. Parler, S.M. Butler, J.R. Miller, Fast Response, Carbon-Black-Coated, Vertically-Oriented Graphene Electric Double Layer Capacitors, J. Electrochem. Soc. 165 (2018) A924-A931.
- [14] G. Ren, X. Pan, S. Bayne, Z. Fan, Kilohertz ultrafast electrochemical supercapacitors based on perpendicularly-oriented graphene grown inside of nickel foam, Carbon 71 (2014) 94-101.
- [15] M. Zhang, Q. Zhou, J. Chen, X. Yu, L. Huang, Y. Li, C. Li, G. Shi, An ultrahigh-rate electrochemical capacitor based on solution-processed highly conductive PEDOT: PSS films for AC line-filtering, Energy Environ Sci. 9 (2016) 2005-2010.
- [16] Y. Rangom, X.S. Tang, L.F. Nazar, Carbon Nanotube-Based Supercapacitors with Excellent ac Line Filtering and Rate Capability via Improved Interfacial Impedance, ACS Nano 9 (2015) 7248-55.
- [17] R. De Levie, On porous electrodes in electrolyte solutions: I. Capacitance effects, Electrochim. Acta 8 (1963) 751-780.

- [18] M.F. El-Kady, V. Strong, S. Dubin, R.B. Kaner, Laser Scribing of High-Performance and Flexible Graphene-Based Electrochemical Capacitors, Science 335 (2012) 1326-1330.
- [19] D. Pech, M. Brunet, H. Durou, P. Huang, V. Mochalin, Y. Gogotsi, P.-L. Taberna, P. Simon, Ultrahigh-power micrometre-sized supercapacitors based on onion-like carbon, Nat. Nanotech. 5 (2010) 651.
- [20] L. Yunyong, L. Zesheng, S.P. Kang, Simultaneous Formation of Ultrahigh Surface Area and Three-Dimensional Hierarchical Porous Graphene-Like Networks for Fast and Highly Stable Supercapacitors, Adv. Mater. 25 (2013) 2474-2480.
- [21] J.R. Miller, R.A. Outlaw, B.C. Holloway, Graphene electric double layer capacitor with ultra-high-power performance, Electrochim. Acta 56 (2011) 10443-10449.
- [22] J.-P. Randin, E. Yeager, Differential capacitance study on the edge orientation of pyrolytic graphite and glassy carbon electrodes, J. Electroanal. Chem. Interfacial Electrochem. 58 (1975) 313-322.
- [23] G. Ren, M.N.F. Hoque, J. Liu, J. Warzywoda, Z. Fan, Perpendicular edge oriented graphene foam supporting orthogonal TiO₂(B) nanosheets as freestanding electrode for lithium ion battery, Nano Energy 21 (2016) 162-171.
- [24] N. Islam, J. Warzywoda, Z. Fan, Edge-Oriented Graphene on Carbon Nanofiber for High-Frequency Supercapacitors, Nano-Micro Letters 10 (2018) 9.
- [25] L. Jiang, G.W. Nelson, H. Kim, I.N. Sim, S.O. Han, J.S. Foord, Cellulose-Derived Supercapacitors from the Carbonisation of Filter Paper, ChemistryOpen 4 (2015) 586-9.
- [26] S. Li, T. Mou, G. Ren, J. Warzywoda, Z. Wei, B. Wang, Z. Fan, Gel based sulfur cathodes with a high sulfur content and large mass loading for high-performance lithium–sulfur batteries, J. Mater. Chem. A 5 (2017) 1650-1657.
- [27] R. Shao, J. Niu, J. Liang, M. Liu, Z. Zhang, M. Dou, Y. Huang, F. Wang, Mesopore- and Macropore-Dominant Nitrogen-Doped Hierarchically Porous Carbons for High-Energy and Ultrafast Supercapacitors in Non-Aqueous Electrolytes, ACS Appl. Mater. Interfaces 9 (2017) 42797-42805.
- [28] W. Zhen-Yu, L. Chao, L. Hai-Wei, C. Jia-Fu, Y. Shu-Hong, Ultralight, Flexible, and Fire-Resistant Carbon Nanofiber Aerogels from Bacterial Cellulose, Angewandte Chem. 125 (2013) 2997-3001.
- [29] S. Li, G. Ren, M.N.F. Hoque, Z. Dong, J. Warzywoda, Z. Fan, Carbonized cellulose paper as an effective interlayer in lithium-sulfur batteries, Appl. Surf. Sci. 396 (2017) 637-643.
- [30] I. Milosavljevic, V. Oja, E.M. Suuberg, Thermal effects in cellulose pyrolysis: relationship to char formation processes, Ind. Eng. Chem. Res. 35 (1996) 653-662.
- [31] N. Islam, S. Wang, J. Warzywoda, Z. Fan, Fast supercapacitors based on vertically oriented MoS2 nanosheets on plasma pyrolyzed cellulose filter paper, J. Power Sources 400 (2018) 277-283.

- [32] J. Zhao, M. Shaygan, J.r. Eckert, M. Meyyappan, M.H. Rümmeli, A growth mechanism for free-standing vertical graphene, Nano Lett. 14 (2014) 3064-3071.
- [33] M. Hiramatsu, K. Shiji, H. Amano, M. Hori, Fabrication of vertically aligned carbon nanowalls using capacitively coupled plasma-enhanced chemical vapor deposition assisted by hydrogen radical injection, Appl. Phys. Lett. 84 (2004) 4708-4710.
- [34] M. Zhu, J. Wang, B.C. Holloway, R. Outlaw, X. Zhao, K. Hou, V. Shutthanandan, D.M. Manos, A mechanism for carbon nanosheet formation, Carbon 45 (2007) 2229-2234.
- [35] Z. Bo, S. Mao, Z.J. Han, K. Cen, J. Chen, K.K. Ostrikov, Emerging energy and environmental applications of vertically-oriented graphenes, Chem. Soc. Rev. 44 (2015) 2108-2121.
- [36] Z. Zhang, W. Li, M.F. Yuen, T.-W. Ng, Y. Tang, C.-S. Lee, X. Chen, W. Zhang, Hierarchical composite structure of few-layers MoS2 nanosheets supported by vertical graphene on carbon cloth for high-performance hydrogen evolution reaction, Nano Energy 18 (2015) 196-204.
- [37] C.J. Garvey, I.H. Parker, G.P. Simon, On the interpretation of X-ray diffraction powder patterns in terms of the nanostructure of cellulose I fibres, Macromol. Chem. Phys. 206 (2005) 1568-1575.
- [38] R.A. Quinlan, M. Cai, R.A. Outlaw, S.M. Butler, J.R. Miller, A.N. Mansour, Investigation of defects generated in vertically oriented graphene, Carbon 64 (2013) 92-100.
- [39] J.-P. Candy, P. Fouilloux, M. Keddam, H. Takenouti, The characterization of porous electrodes by impedance measurements, Electrochim. Acta 26 (1981) 1029-1034.
- [40] M. Cai, R.A. Outlaw, S.M. Butler, J.R. Miller, A high density of vertically-oriented graphenes for use in electric double layer capacitors, Carbon 50 (2012) 5481-5488.
- [41] G. Ren, S. Li, Z.-X. Fan, M.N.F. Hoque, Z. Fan, Ultrahigh-rate supercapacitors with large capacitance based on edge oriented graphene coated carbonized cellulous paper as flexible freestanding electrodes, J. Power Sources 325 (2016) 152-160.
- [42] J.R. Miller, R.A. Outlaw, Vertically-oriented graphene electric double layer capacitor designs, J. Electrochem. Soc. 162 (2015) A5077-A5082.
- [43] R. Kötz, M. Carlen, Principles and applications of electrochemical capacitors, Electrochim. Acta 45 (2000) 2483-2498.
- [44] J. Lin, C. Zhang, Z. Yan, Y. Zhu, Z. Peng, R.H. Hauge, D. Natelson, J.M. Tour, 3-Dimensional graphene carbon nanotube carpet-based microsupercapacitors with high electrochemical performance, Nano Lett. 13 (2013) 72-8.
- [45] P.L. Taberna, P. Simon, J.F. Fauvarque, Electrochemical Characteristics and Impedance Spectroscopy Studies of Carbon-Carbon Supercapacitors, J. Electrochem. Soc. 150 (2003) A292.

- [46] R.J. Gilliam, J.W. Graydon, D.W. Kirk, S.J. Thorpe, A review of specific conductivities of potassium hydroxide solutions for various concentrations and temperatures, Int. J. Hydrog. Energy 32 (2007) 359-364.
- [47] C. Zhong, Y. Deng, W. Hu, J. Qiao, L. Zhang, J. Zhang, A review of electrolyte materials and compositions for electrochemical supercapacitors, Chem. Soc. Rev. 44 (2015) 7484-7539.
- [48] M.H. Ervin, C.M. Pereira, J.R. Miller, R.A. Outlaw, J. Rastegar, R.T. Murray, Graphene-Based and Other Electrochemical Double Layer Capacitors for Energy Harvesting Systems, ECS J. Solid State Sci. Technol. 2 (2013) M3135-M3139.